Journal of Radioanalytical and Nuclear Chemistry (2024) 333:4091–4106
https://doi.org/10.1007/s10967-024-09563-x

Research on urease-modified *Deinococcus radiodurans* and the control mechanism of the contamination of U(VI)

Yujin Liang[1] · Kexin Guo[1] · Fan Jiang[1] · Guowen Peng[2] · Fangzhu Xiao[1]

Received: 22 February 2024 / Accepted: 17 May 2024 / Published online: 7 June 2024

Abstract

Biosorption by microorganisms is an environmentally friendly and efficient method to adsorb heavy metals and radionucleids. The purpose of this study was to transform urease gene (*Ure*) from *Sporosarcina pasteurii DSM33* into *D.radiodurans* to prepare a recombinant Deino-*Ure* strains. The urease was used to decompose urea to produce CO_3^{2-}, promoting calcium carbonate precipitation in the presence of Ca^{2+}. This enhances the biomineralisation and U(IV) enrichment of *D. radiodurans*, which provides a scientific basis for the treatment of low enriched uranium contaminated soil. During Deino-*Ure* mineralization of U(VI), uranium may co-precipitate with calcium, forming a stable U(VI)/U (IV)-calcite mineral precipitate.

Keywords *Deinococcus radiodurans* · Uranium · Urease · Biomineralization · Microbially induced carbonate precipitation

Introduction

As one of the most significant basements of human well-being, soil has been contaminated by the undue disposition of pesticides and industrial wastewater, waste gases, and residues, resulting in an increasingly severe pollution issue in the soil and gravely threatening public health and food security [1–4]. Thereinto, a hot and difficulty issue lie in the control and prevention of radionuclide pollution in soils, especially the remediation of soil in uranium mining and metallurgical areas, which urgently requires solving [5–7]. While the uranium in soil could be absorbed into plants by rhizomes and eventually ingested by the human body through the food chain. In addition, edaphic uranium could constantly migrate downward and spread during hydrological changes such as rainfall and irrigation, entering the groundwater cycle and causing more extensive pollution. If the diffused uranium is ingested or inhaled into the human body, it will trigger a permanent and strong internal radiation that is extremely harmful and may induce cancer [8, 9].

Contemporary remediation technology for contaminated soil consists of physical remediation, chemical remediation, and biological remediation [10, 11], and biomineralization is a inseparable part of biological remediation. Microbially induced carbonate precipitation (MICP), a remediation method to treat metallic contamination proposed in recent years [12–14], is mainly based on the decomposition of urea by urease secreted by carbonate-mineralizing bacteria to produce carbonate that could form precipitation in the presence of Ca^{2+} or other metal ions [15, 16]. *Sporosarcina pasteurii* (*S. pasteurii*) possesses favorable secretory ability of urease and a multitude of studies have shown that it also has satisfactory urease activity about 100 times that of soybean urease and 14 folds that of Jack bean urease [17, 18]. Thus, *S. pasteurii* is employed as a common strain for bio-induced calcium carbonate mineralization and has been progressively utilized in the fields of architecture, environment, and even medical treatment [19–21]. However, most of carbonate-mineralizing bacteria may be inherently devoid of tolerance for radionuclides, making it difficult to achieve pleasing results in practical applications. While *D.radiodurans* is known as the "most resistant bacterium in the world", which can survive in a high-intensity radioactive environment, exhibiting great prospects for exploitation [22]. According

Yujin Liang and Kexin Guo have contributed equally to this work and should be considered co-first authors.

✉ Guowen Peng
pgwnh78@163.com

✉ Fangzhu Xiao
xfzhunh@163.com

[1] School of Public Health, University of South China, Hengyang 421001, China

[2] School of Resources Environment and Safety Engineering, University of South China, Hengyang 421001, China

to previous researches, the urease gene cluster of *S. pasteurii* can be successfully heterologously expressed in other hosts and obtain comparable urease activity to *S. pasteurii* [23]. Herein, we managed to transfer the urease gene of *S. pasteurii* into *D.radiodurans* for stable expression and link the optimized fragment to the *E. coli* shuttle plasmid (pRADK) to construct the pRADK-*Ure* plasmid vector, which was transferred into *D.radiodurans* in order to acquire a genetically engineered bacterium with both radiation resistance and prominent biomineralization ability, providing theoretical and experimental support for slowing down the migration of nuclear waste in the environment and the microbial treatment of uranium-containing soil.

Material and methods

Bacterial strains and growth conditions

Bacterial strains, primers and plasmids used in this study were listed in Table 1. *E. coli* shuttle plasmid (pRADK) was funded by Yuejin Hua group and *D.radiodurans* R1 was preserved in our laboratory. *D.radiodurans* R1 was cultured with TGY solid medium at 30 ± 1 °C and 220 rpm. TGY liquid medium was prepared with 0.5% tryptone, 0.1% glucose, and 0.3% yeast extract, while TGY solid medium was manufactured with liquid medium plus 1.5% agar.

Construction of genetically engineered *D.radiodurans* containing urease gene clusters

The target gene was designed according to the urease gene cluster sequence *UreABCDEFGD* of *S. pasteurii DSM33* strain in the NCBI database. Urease expression has been shown to be enhanced by adjusting the large subunit *UreC* in the urease gene cluster upstream of *UreA* and *UreB* [24, 25]. Therefore, in this experiment, before the large subunit *UreC* gene was moved to *UreA* and *UreB* genes, the codon and ribosome binding sites of the target gene sequence were optimized by Tsingke Biotech Co., Ltd. to synthesize the whole *UreCABEFGD* gene (hereinafter referred to as *Ure* gene) [26–28]. The synthesized *Ure* gene was used as a template, and the designed precursors of *Ure-F* and *Ure-R* were added to manipulate the polymerase chain reaction in order to amplify *Ure* gene fragment with NdeI and BstEII enzymatic cleavage sites. coli-D. The *Ure* gene was cloned downstream of the strong promoter of *D.radiodurans* to construct the recombinant plasmid pRADK-*Ure*. Finally, the recombinant plasmid pRADK-*Ure* was transformed into *D.radiodurans* cells, and positive clones were screened on TGY agar medium containing 3.4 μg/ml of chloramphenicol.

Table 1 Bacterial strains, plasmids, and primers used in this study

Strains, plasmids and primers	Description	Source, reference or comment
Strains		
D.radiodurans R1		lab collection
pRADK	*D.radiodurans-E. coli* shuttle vector, 7.9 kb, containing Amp, Kana and Cm resistance, with *D. deinococcal* groEL promoter	lab collection
Primers		
Ure-F	5'CATATGCACCACCACCACCACCACG(NdeI)	Nanjing Tsingke Biotech Co., Ltd
Ure-R	5'GGTAACCTCACACGATGTAGTTGGC(BstEII)	
UreA-F	5'CTGCACCTGAACCCCGCCG	
UreA-R	5'TCAGCTGATGGGGTTGTGCACGG	
UreB-F	5'GTGTCGAACAACAACTACATCGTGC	
UreB-R	5'TCATTCCACGCCCTTGTAGC	
UreC-F	5'GTGAAGATCAACCGCCAGCAG	
UreC-R	5'TCAGAACAGGAAGTAGCGCTG	
UreD-F	5'ATGGAGTTCCAGTACCGCGG	
UreD-R	5'TCACACGATGTAGTTGGCGAAC	
UreE-F	5'ATGCTGCTCATCACCAAGATCGTGGG	
UreE-R	5'TCAGTGCTGGTGGCCGCG	
UreF-F	5'ATGGAGACCTACATCCAGGAGAGC	
UreF-R	5'TCAGCTGATGAAGAGGCGCG	
UreG-F	5'ATGAAGACCATCCACCTGGGCATCG	
UreG-R	5'TCACTTGCTCTCGCTGGCGC	

Determination of urease activity and calcium carbonate yield

In this experiment, urease activity was measured by the electrical conductivity method and the indophenol blue colorimetric method. Urea is non-conductive, while the urease produced by bacteria could hydrolyze urea to generate conductive NH_4^+ and CO_3^{2-}. The increase in conductivity of the detected solution was positively correlated to the amount of hydrolyzed urea, and the relationship between the two was as given in Eq. (1) [29]:

$$\begin{aligned}&\text{hydrolyzed urea (mmol/L)}\\&\quad = \text{conductivity change (ms/cm)}\\&\quad \times 11.11\left(R^2 = 0.9988\right)\end{aligned} \tag{1}$$

The produced NH_4^+ in the urea hydrolysis process could react with phenol-sodium hypochlorite to form indophenol, which could increase the absorbance value at 625 nm. Thus the generated NH_4^+ could be quantitated by measuring the degree of the chromegenic reaction in order to calculate the microbial urease activity [30]. Moreover, 1 mL of Deino-*Ure* bacterial solution of different concentrations was added into a mixture containing 0.5 mol/L of urea and 0.5 mol/L of $CaCO_3$, and the calcium carbonate yield was measured in different reaction time periods. The mixed solution was filtered with paper filters, washed with ultrapure water, and dried. Subsequently, 0.1 mol/L of HCl solution was added to wash multiple times until no bubbles were formed, washed with ultrapure water, and dried, then weighed, and the calcium carbonate yield was calculated as the difference between the two readings.

Experimental design using response surface methodology

To explore the effects of different Ni^{2+}, Ca^{2+}, and urea concentrations on the urease activity of the recombinant strain Deino-*Ure*, the optimal design using the Box-Behnken response surface model was analyzed by Design-Expert 12 software. Taking the urease activity and calcium carbonate yield of the recombinant strain as the response surfaces and values, concentrations of Ni^{2+} (A), urea (B), and Ca^{2+} (C) were designed to optimize the response surface, and the optimal conditions for the urease activity and calcium carbonate yield of the recombinant deino-ure strain were calculated through simulation analysis (Table 2).

Uranium mineralization enrichment experiment

A certain amount of bacterial solution was centrifuged, and the medium was discarded. Then an equal volume of 0.9% NaCl was added to resuspend the bacteria. Subsequently, the bacterial suspension was mixed with uranium solution, urea solution, Ca^{2+} solution, and Ni^{2+} solution, and the pH of the mixture was adjusted by NaOH and HCl. Furthermore, 0.9% NaCl was added to make the final concentrations of urea, Ca^{2+}, and Ni^{2+} 30 g/L, 10 g/L, and 0.5 mol/L, respectively. Finally, the uranium mineralization enrichment experiment was carried out at 30 °C and 220 rpm. After the mineralization was completed, the concentration of uranium in the centrifugal supernatant was determined by the value change of absorbance of azoarsine (III) method at 652 nm [31] to calculate the enrichment rate (R) as given in Eq. (2)

$$R = \left(C_0 - C_t\right)/C_0 \times 100\% \tag{2}$$

R (%) represented the enrichment rate of uranium, C_0 indicated the initial concentration of uranium, and C_t served as the remaining concentration of uranium in solution after the time of uranium enrichment.

Table 2 Designed factor level of Box–Behnken experiment

Factors	Levels		
	−1	0	1
A:Ni^{2+} concentration(mmol/L)	0.25	0.5	0.75
B:Urea concentration(g/L)	20	30	40
C:Ca^{2+} concentration(g/L)	5	10	15

Scanning electron microscopy (SEM), Energy dispersive spectrometer (EDS), X-ray photoelectron spectroscopy (XPS) and X-ray diffraction (XRD) of mineralised Deino-*Ure* cells

30 mL of the solution before and after the mineralization experiment was transferred to a 50 mL centrifuge tube and centrifuged at 4000 rpm for 10 min. Then the supernatant was discarded, and the precipitate was dried at 65 °C for 24 h to remove water. After cooling down, the dried solids were scraped off and ground into powder in a mortar, weighed, and placed in a 1.5-mL EP tube for later SEM, EDS, XPS, and XRD analysis experiments.

Results and discussion

Identification of the recombination strain Deino-*Ure*

Single colony of *D.radiodurans* was picked from TGY solid medium plate with 3.4 μg/mL chloramphenicol and cultured. Then the plasmid was extracted for PCR experiment, and the results were shown in Fig. 1. In the first lane, the bands matching the size of the target genes were exhibited (303 bp

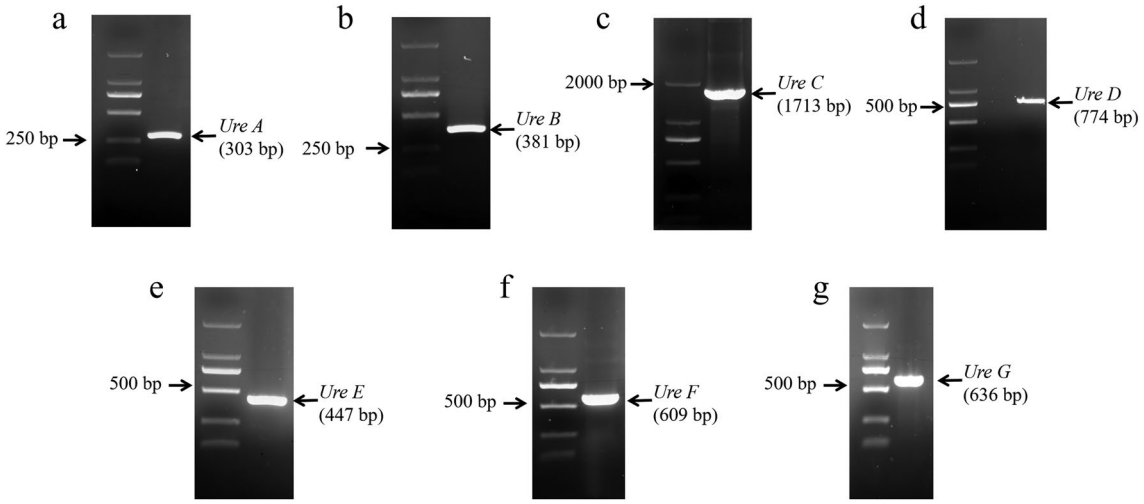

Fig. 1 The PCR results of recombinant plasmid pRADK-*Ure*. PCR amplification products of *UreA, B, C, D, E, F,* and *G* genes; Line M: DNA Marker; Line 1: *UreA, B, C, D, E, F, G* gene PCR amplification products

of *UreA*, 381 bp of *UreB*, 1713 bp of *UreC*, 774 bp of *UreD*, 447 bp of *UreE*, 609 bp of *UreF*, and 636 bp of *UreG*, respectively), indicating that the recombinant plasmid pRADK-*Ure* had been successfully transformed into *D.radiodurans*. Then the PCR products were sequenced and compared by NCBI's nucleic acid Blast alignment, which illustrated that the pRADK-Ure recombinant plasmid had been successfully transferred into *D.radiodurans* to construct a genetically engineered bacterium with radiation tolerance and the urease gene *Ure*.

Study on the growth and urease activity of Deino-*Ure*

Single colonies of wild *D.radiodurans* and Deino-*Ure* recombinant strains on TGY solid medium were selected and cultured to OD_{600}≈1 at 30 °C in TGY liquid medium. Then bacterial solutions were transferred to fresh TGY liquid with an inoculum size of 2%. OD_{600} was measured every 2 h to obtain growth curves for Deino-*wt* and Deino-*Ure*, as shown in Fig. 2. The result illustrated that the growth curves of Deino-*wt* and Deino-*Ure* were highly overlapping and there was no significant difference, indicating that the *Ure* gene would not affect the growth of recombinant strains.

1.5 mL of different OD_{600} solutions were added to 13.5 mL of 0.5 M urea solution, and the conductivity of the mixture was measured at certain intervals. As elucidated in Fig. 3a, the increase in bacterial concentration could significantly accelerate the urea hydrolysis proces**s,**

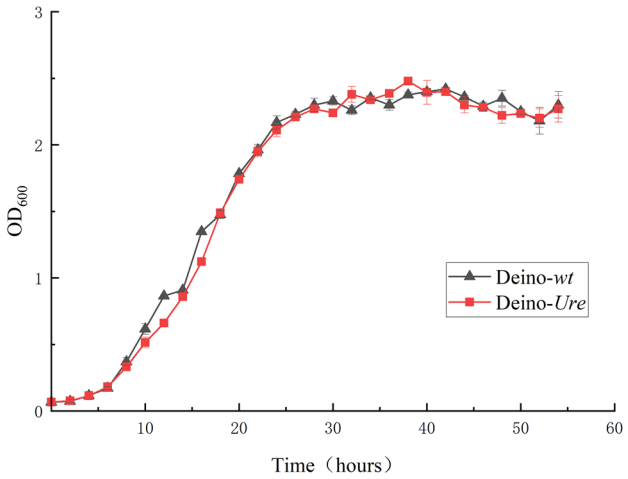

Fig. 2 Growth curves of Deino-*wt* and Deino-*Ure*

and the decomposition rate of urea was the fastest when the OD_{600} of the bacterial solution equaled 1.0. In addition, the conductivity of the four concentrations reached a peak at about 72 h, indicating that the urea in the solution had been completely decomposed at this time. The yield of $CaCO_3$ increased with the increase in bacterial concentrations (Fig. 3b), reached a higher value within 3 days with the increase in reaction time, and then slowly and gradually increased. Therefore, increasing the concentration of bacteria at a certain concentration of urea and Ca^{2+} could effectively enhance the production of $CaCO_3$.

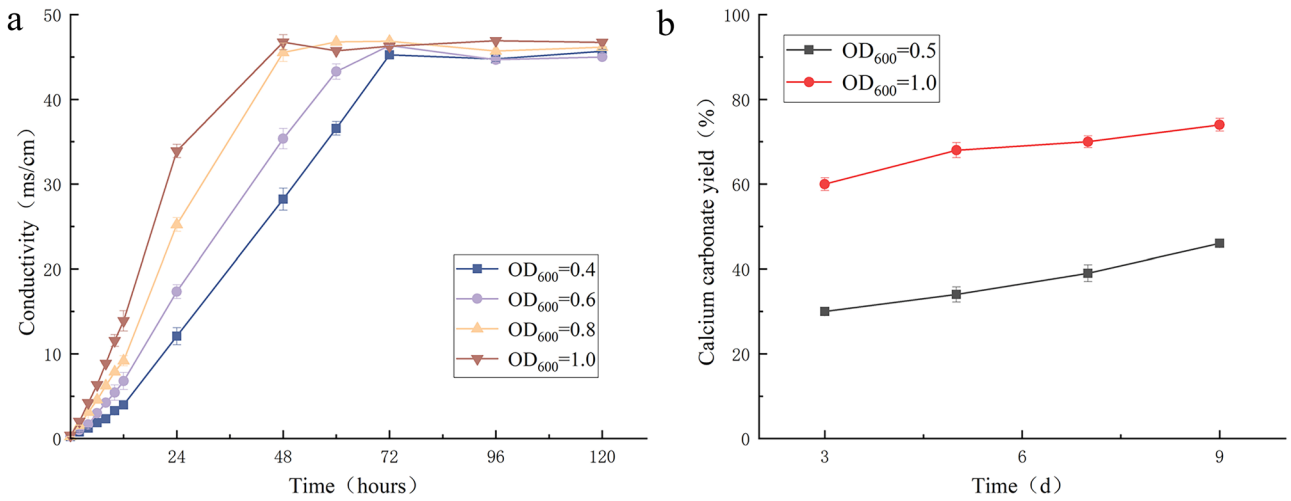

Fig. 3 Changes of conductivity and calcium carbonate yield at different bacterial concentrations. **a** Changes of conductivity at different bacterial concentrations; **b** Yield of calcium carbonate with different bacterial, concentrations

Effects of different substrate concentrations on the growth and urease activity of recombinant bacteria Deino-*Ure*

Effect of Ni^{2+} concentration on the growth and urease activity of Deino-*Ure*

Urease is a metal-dependent enzyme whose active center requires the involvement of Ni^{2+} [32, 33]. The growth curve and urease activity of the recombinant strain Deino-*Ure* under different concentrations of Ni^{2+} were exhibited in Fig. 4. With the increase in Ni^{2+} concentration, the OD_{600} value of the recombinant bacteria and the growth rate decreased significantly, and the recombinant bacteria could hardly grow when the concentration of Ni^{2+} reached 1 mmol/L. However, as presented in Fig. 4b, Ni^{2+} played a significant role in enzyme activity, and with the increase in Ni^{2+} concentration, urease activity increased significantly, reaching a peak at 0.5 mmol/L of Ni^{2+}. When Ni^{2+} surpassed 0.5 mmol/L, urease activity could decrease. Combined with the growth curve of Ni^{2+} concentration, it was inferred that the appropriate concentration of Ni^{2+} could be conducive to the production of active urease by Deino-Ure, while the decrease in urease activity may be due to the cytotoxicity and the inhibitory effect on the growth of recombinant bacteria caused by the overly high level of nickel [34, 35]. Therefore, 0.5 mmol/L of Ni^{2+} was determined to be the optimal condition for the following mineralization.

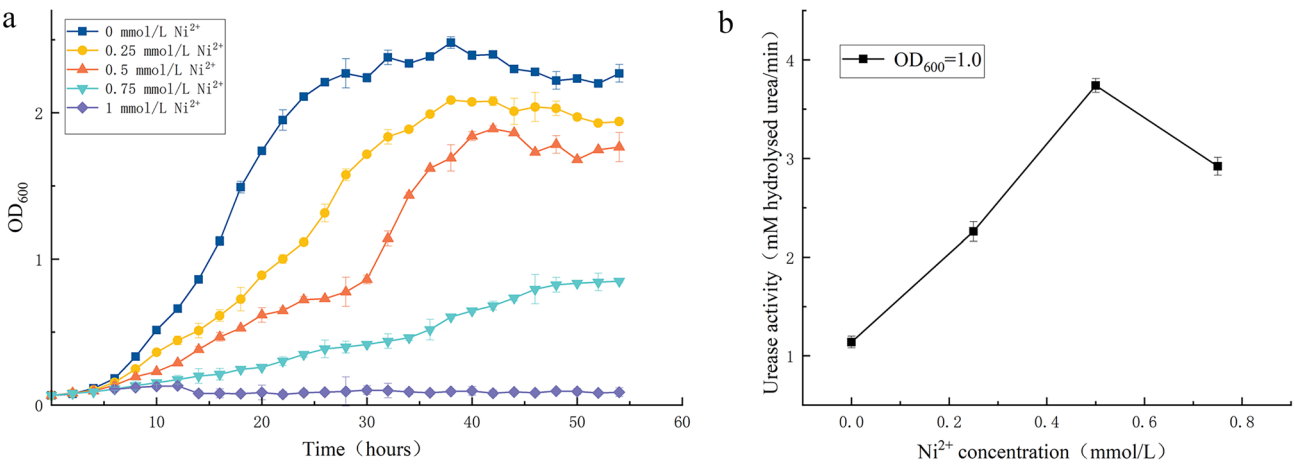

Fig. 4 Growth curve and urease activity at different concentrations of Ni^{2+} **a** Growth curves at different concentrations of Ni^{2+}; **b** Urease activity at different concentrations of Ni^{2+}

Effect of urea concentration on growth and urease activity of Deino-*Ure*

Urea is an essential substrate for MICP, which could provide carbon and nitrogen source for bacteria, but excessive concentration of it could also reduce the deposition efficiency of MICP. As shown in Fig. 5a, when the urea concentration exceeded a certain range, the growth of recombinant strains was inhibited, which might be attributed to a large amount of CO_3^{2-} and NH_4^+ produced by the excessively hydrolyzed urea, which could affect the ion balance in the intracellular and extracellular environment and raise the pH, which was not conducive to the survival of bacteria. The urease activity at different urea concentrations was illustrated in Fig. 5b. The urease activity of the strain increased significantly with the increase in urea concentration, and when the urea concentration was 30 g/L, the urease activity reached a maximum value of 3.74 mmol/L hydrolyzed urea/min. Combined with the growth curve of urea concentration, 30 g/L of urea was selected as the optimal mineralization condition.

Effect of Ca^{2+} concentration on growth and urease activity of Deino-*Ure*

In the process of MICP, the concentration of Ca^{2+} has a great influence on the growth of strains and the precipitation amount of calcium carbonate [36], because Ca^{2+} continuously reacts with CO_3^{2-} to form $CaCO_3$ precipitation during the reaction, which will affect the change in conductivity, so the concentration change of NH_4^+–N was determined by the indigophenol blue colorimetric method to reflect the urease activity. Figure 6 presented that high concentrations of Ca^{2+} had a significant inhibitory effect on urease activity, attributable to the fact that Ca^{2+} could change the permeability of bacteria, which was embodied in the preparation of competent cells [37]. In addition, Ca^{2+} functioned as a second messenger in cells to promote or regulate a variety of biochemical activities [38], while

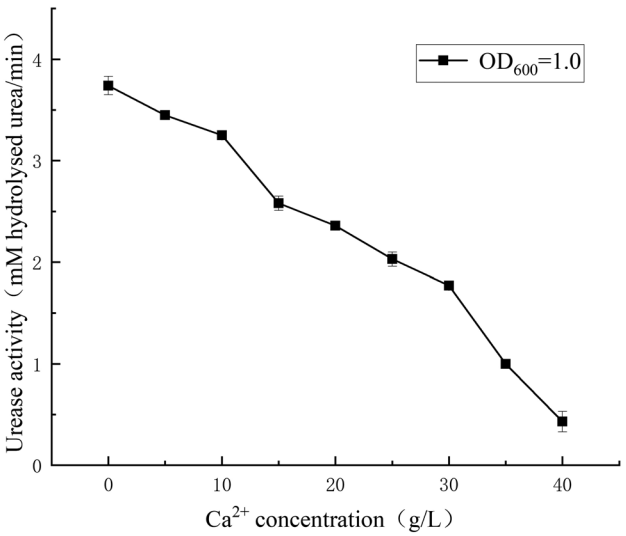

Fig. 6 Urease activity at different concentrations of Ca^{2+}

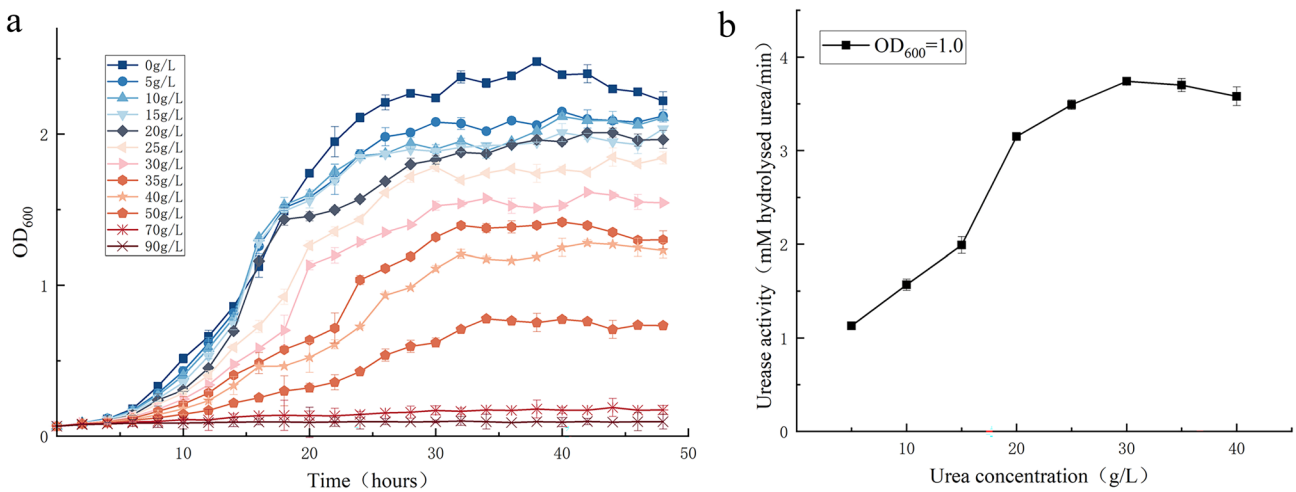

Fig. 5 Growth curve and urease activity at different concentrations of urea. **a** Growth curves at different concentrations of urea; **b** Urease activity at different concentrations of urea

excessive amounts of calcium ions will lead to intracellular calcium overload, resulting in irreversible damage to cells and ultimately apoptosis [39, 40]. Therefore, the optimal mineralization condition of Ca^{2+} concentration was set at 10 g/L in subsequent experiments.

Urease activity and calcium carbonate yield of recombinant strain optimized by the response surface

Urease activity According to the 17 sets of experiments simulated by Design-Expert 12 software and the linear fitting of multiple regression from the experimental data in Table 3, the linear equation of multiple regression of urease activity was obtained as Eq. (3):

$$Y = -6.45 + 20.68A + 0.25B + 0.16C + 0.003AB - 0.024AC + 0.00075BC - 19.25A^2 - 0.004B^2 - 0.014C^2 \quad (3)$$

According to the results of ANOVA (Table 4), A, B, and C all showed extremely significant effects on urease activity ($P < 0.01$), and the single factor effect was $Ca^{2+} > Ni^{2+} >$ urea, with $F = 91.28$ and $P < 0.01$ indicating that the regression equation model fitted well in the entire studied regression region. Moreover, the complex correlation coefficient $R^2 = 0.9916$ inferred that the regression equation model had a good correlation, and the corrected absolute coefficient $Rad_j^2 = 0.9938$ informed that 98.07% of the variability of the experimental data could be explained by this regression model. Therefore, the model of the obtained experiments was reasonable, and it could be used to analyze and predict urease activity.

With an elliptical shape, the contour shape of Fig. 7 showed vertices in both the response surface and the contour map, indicating that there were extreme values in the selected range and that the interaction between Ca^{2+} concentration, Ni^{2+} concentration, and urea concentration was significant, which was basically consistent with the results of ANOVA. Through the analysis of the response surface and contour map, the regression model was calculated, and the optimal conditions for predicting urease activity were $Ca^{2+} = 7.86$ g/L, $Ni^{2+} = 0.54$ mmol/L, and urea = 32.67 g/L, with the urease activity calculated to be 3.54 mmol/L hydrolyzed urea/min.

Calcium carbonate yield According to Design-Expert 12 and the fitting of the experimental data in Table 3, the multiple regression linear equation of calcium carbonate yield was obtained as Eq. (4):

$$Y = -257.75 + 613.8A + 6.768B + 11.215C + 0.4AB + 3.2AC + 0.25BC - 594.8A^2 - 0.104B^2 - 0.697C^2 \quad (4)$$

From the ANOVA results (Table 5), A,B,C showed significant effects on calcium carbonate yield ($P < 0.05$), indicating that Ca^{2+}, Ni^{2+}, and urea concentration are important key control factors for calcium carbonate yield. By analysing the response surface and contour map of the interaction of each response factor on calcium carbonate yield (Fig. 8), and combining with the software to calculate the regression

Table 3 Response surface experimental design and results of urease activity and calcium carbonate yield

Serial number	Ni^{2+} concentration A	Urea concentration B	Ca^{2+} concentration C	Urease activity mM hydrolysed urea/min	$CaCO_3$ productivity%
1	0	−1	−1	3.01	48
2	1	0	1	1.52	46
3	1	0	−1	2.67	40
4	0	1	1	2.19	62
5	0	0	0	3.25	81
6	0	0	0	3.51	83
7	−1	0	−1	1.96	16
8	−1	−1	0	1.25	10
9	−1	0	1	0.93	6
10	0	−1	1	1.76	40
11	0	1	−1	3.29	65
12	0	0	0	3.46	85
13	1	−1	0	1.87	39
14	1	1	0	2.19	60
15	−1	1	0	1.54	27
16	0	0	0	3.15	79
17	0	0	0	3.26	80

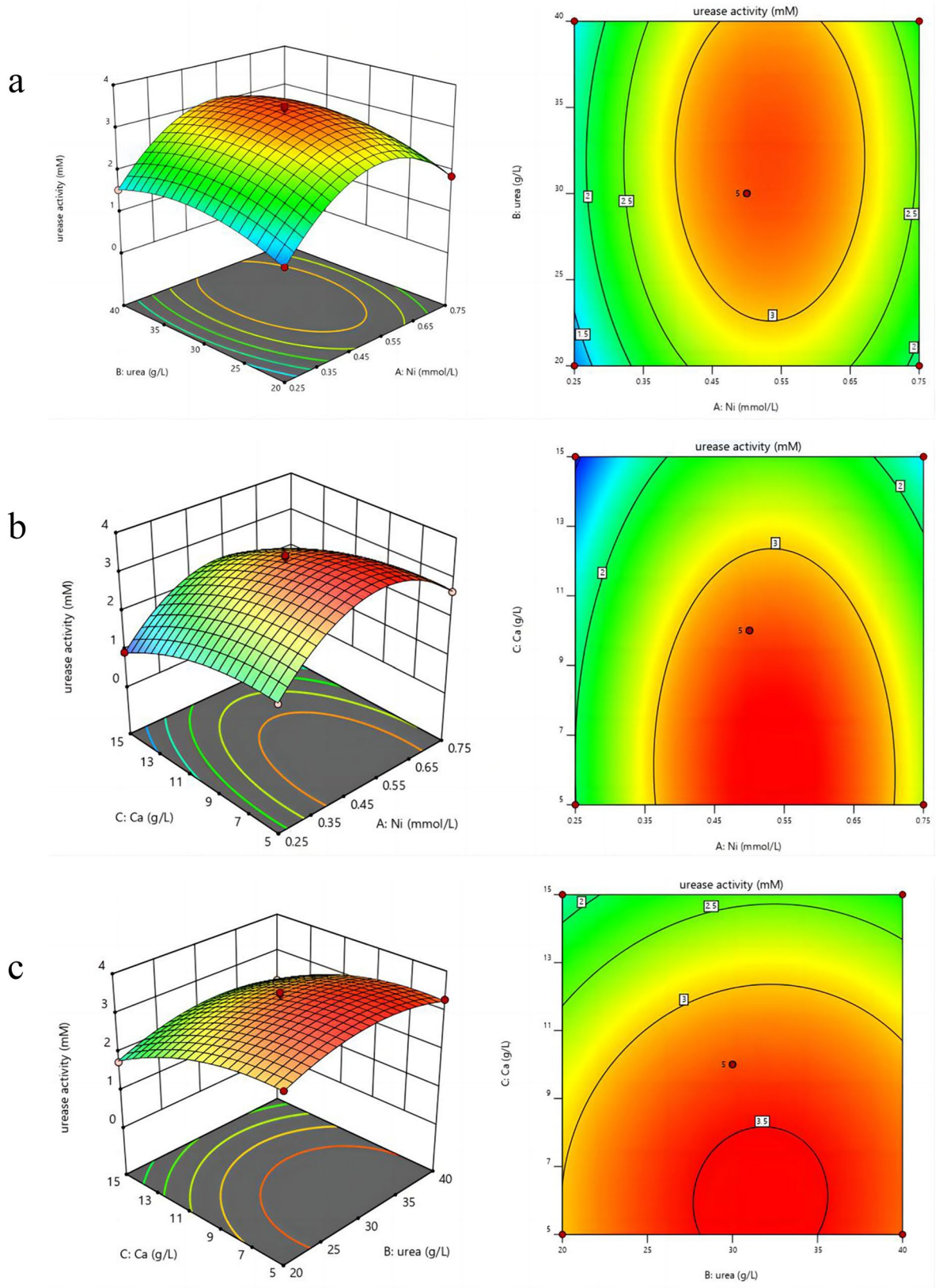

Fig. 7 Effect of interaction of various factors on urease activity. **a** Response surface curves and contour plots of urea concentration and Ni^{2+} concentration on urease activity, **b** Response surface curves and contour plots of Ca^{2+} and Ni^{2+} concentrations on urease activity, **c** Response surface curves and contour plots of Ca^{2+} and urea concentration on urease activity

model can be predicted that the optimal conditions for urease activity are when the $Ca^{2+} = 9.86$ g/L, $Ni^{2+} = 0.54$ mmol/L, and urea = 34.65 g/L. By substituting the three factors into the regression equation, it was calculated that at this time, the calcium carbonate yield was 85.59%.

Comparison of urease activity and calcium carbonate yield under different conditions In light of Design-Expert 12, the optimal urease activity was analyzed under the following conditions: concentrations of Ca^{2+}, Ni^{2+}, and urea were 7.86 g/L, 0.54 mmol/L, and 32.67 g/L, respectively. The conditions for the optimal calcium carbonate yield were 9.86 g/L of Ca^{2+}, 0.54 mmol/L for Ni^{2+}, and 34.65 g/L for urea. Considering the limitations of the experimental conditions, the experimental conditions of the former were adjusted to 0.5 mmol/L of Ni^{2+}, 33 g/L of urea, and 8 g/L of Ca^{2+}, and those of the latter were adjusted to 0.5 mmol/L, 35 g/L, and 10 g/L for Ni^{2+}, urea, and Ca^{2+}, respectively. Under these conditions, urease activities were 3.5 ± 0.05 mmol/L hydrolyzed urea/min and 3.5 ± 0.01 mmol/L hydrolyzed urea/min, respectively, and the calcium carbonate yields were $82 \pm 1\%$ and $85 \pm 0.6\%$, respectively. The experimental results were close to the theoretical values, indicating that the model was reliable and suitable for the optimization of urease activity and calcium carbonate yield.

Based on the above results, 0.5 mmol/L of Ni^{2+}, 35 g/L of urea, and 10 g/L of Ca^{2+}, were selected as the subsequent mineralization experimental conditions (Table 4).

Effects on minerilization of uranium by Denio-*Ure*. Shaking flask experiments were utilized to investigate the effects of changes in time, pH, and initial uranium concentration on the uranium mineralized by Deino-*Ure*, as shown in Figs. 9, 10, 11. On the first day of enrichment (Fig. 9), both Deino-*wt* and Deino-*Ure* provided extremely fast rates of enriching uranium, slowing down over time without significant change in uranium concentrations beyond the second day, possibly due to the large number of available adsorption sites on the surface of both bacteria at the beginning of enrichment to bind uranium to their surfaces. With the passage of time, the adsorption sites on the surface of Deino-*wt* decreased until they were completely occupied and finally reached enrichment equilibrium, with a maximum enrichment rate of only 70%. However, the Deino-*Ure* strain did not reach the enrichment equilibrium until the seventh day, which might be due to the fact that the urease produced by Deino-*Ure* continuously decomposed the urea in the solution environment to produce carbonate ions and formed calcium carbonate precipitation with Ca^{2+} in the solution, which promoted the continuous co-precipitation of uranium and calcium with a maximum enrichment rate of 90%.

pH could affect the mineralization process by influencing the chemical properties (charge distribution) of uranium and the urease activity of Deino-*ure*. The results (Fig. 10) showed that the Deino-*Ure* strain had a high level of uranium mineralization efficiency in the pH range of 6 ~ 9, with a maximum enrichment rate of 90%, indicating that it was more prone to mineralization under alkaline conditions, which might be attributable to the optimal pH range of bacterial urease in the pH range of 6 ~ 9, in which it could exert its best activity [41]. Meanwhile, H^+ in the acidic environment could produce an acid–base neutralization reaction with carbonate and ammonia, which was not conducive to the formation of calcium carbonate crystals (Table 5).

Finally, the effect of different initial uranium concentrations on the mineralized uranium of radiation-tolerant *D.radiodurans* Deino-*Ure* was investigated, and the results were stated in Fig. 11. When the initial concentrations of uranium were 20 mg/L and 30 mg/L, the uranium mineralization efficiency was higher, which may be due to the fact that when the initial concentration of uranium was low, the solution contained fewer uranyl ions, so there was enough Ca^{2+} in the solution to support the continuous co-precipitation of uranium and calcium, triggering higher mineralization efficiency. With the increase in the initial concentration of uranium, the amount of Ca^{2+} in the solution remained unchanged, and when Ca^{2+} in the solution was consumed, the uranium mineralization efficiency gradually decreased with the increase in the amount of uranyl remaining in the solution. In addition, due to the radiation resistance of DR, the enrichment rate of uranium was still more than 60% when the uranium concentration was high, which had important potential value in exploring the bioaccumulation of high-concentration uranium wastewater.

SEM, EDS, XPS, and XRD analyses Figure 12 verbalized the SEM images of the samples before and after the mineralization experiment. Before the experiment, the surface of the

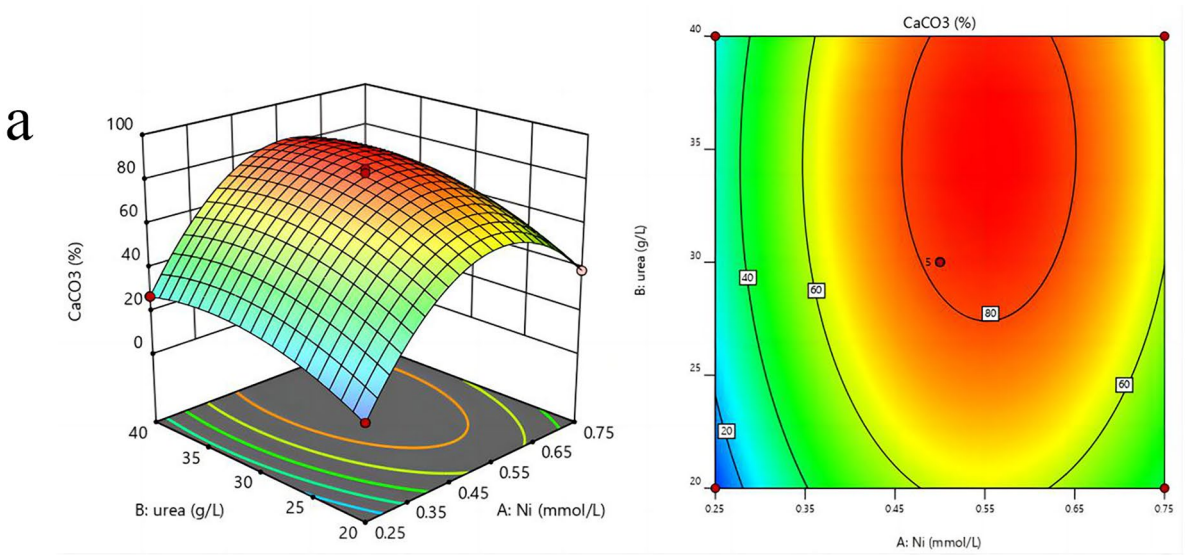
a
CaCO3 (%)
B: urea (g/L)
A: Ni (mmol/L)
CaCO3 (%)
B: urea (g/L)
A: Ni (mmol/L)

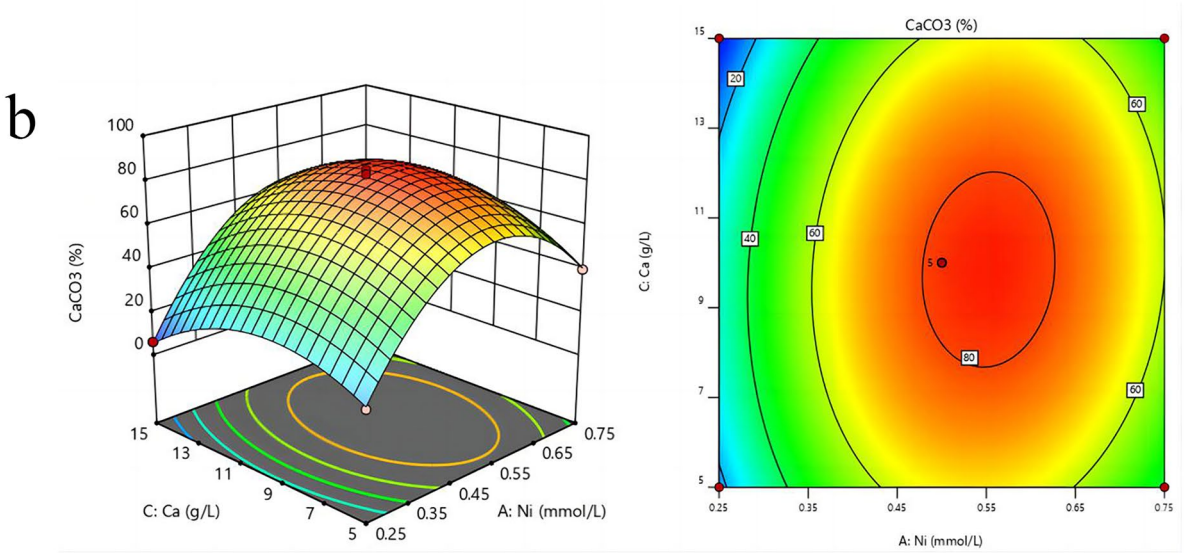
b
CaCO3 (%)
C: Ca (g/L)
A: Ni (mmol/L)
CaCO3 (%)
C: Ca (g/L)
A: Ni (mmol/L)

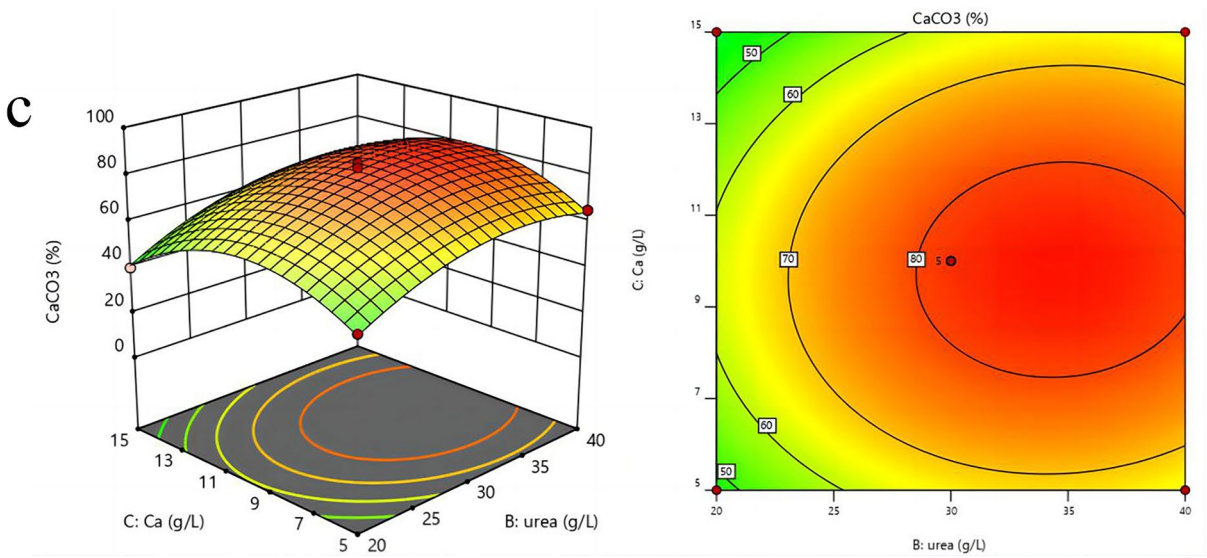
c
CaCO3 (%)
C: Ca (g/L)
B: urea (g/L)
CaCO3 (%)
C: Ca (g/L)
B: urea (g/L)

◂**Fig. 8** Effect of interaction of various factors on calcium carbonate yield. **a** Response surface curves and contour plots of urea concentration and Ni^{2+} concentration on calcium carbonate yield, **b** Response surface curves and contour plots of Ca^{2+} and Ni^{2+} concentrations on calcium carbonate yield, **c** Response surface curves and contour plots of Ca^{2+} and urea concentration on calcium carbonate yield

sample was relatively smooth and flat (a). After mineralization, the morphology changed gravely. The surface structure of the bacteria was destroyed, and clear patterns of crystals appeared on the surface after mineralization (b–c). Calcium carbonate is generally divided into three crystal forms: rhombohedral calcite, rod-shaped aragonite, and spherical vaterite. Calcite is the most stable form. As exhibited in the figure, clear crystals appeared after mineralization, among which were similar to the globular configuration of vaterite and the tetrahedral configuration of calcite.

The EDS spectra of the Deino-*Ure* recombinant strain before and after uranium mineralization (Fig. 13) elucidated that the recombinant Deino-*Ure* strain after mineralization presented obvious medium calcium and uranium peaks at a binding energy of 3 ~ 4 keV (Fig. 13b), confirming that uranium ions could enter the lattice of calcium carbonate to occupy the Ca^{2+} position and form $(U,Ca)CO_3$ crystals.

In order to further study the mechanism of uranium mineralization by Deino-*Ure*, XRD analysis was performed. The results in Fig. 14 illustrated that the sample after mineralization of U(VI) by Deino-*Ure* contained Ca, U, and O (A), proving that the sample might be a combination mineral of Ca, U, and O elements. (B) is the U4f spectrum after Deino-*Ure* mineralized U(VI). The $U4f_{5/2}$ peak appeared at 388.26 eV, and the $U4f_{7/2}$ peak was exhibited at 384.37 eV. The peaks of $U4f_{5/2}$ peak at 391.98 eV and $U4f_{7/2}$ peak at 384.78 eV were represented as U(VI), and the peaks of $U4f_{5/2}$ peak and $U4f_{7/2}$ peak at 388.67 eV and 380.98 eV

Table 4 Variance analysis of urease activity by response surface model

Source of variance	Sum of square	Degree of freedom	Mean square	F value	*P* value	Significance
Model	11.49	9	1.28	91.28	< 0.0001	**
A:Ni^{2+} concentration	0.83	1	0.83	59.0356	0.0001	**
B:Urea concentration	0.2178	1	0.2178	15.5738	0.0056	**
C:Ca^{2+} concentration	2.5651	1	2.5651	183.4188	< 0.0001	**
AB	0.0002	1	0.0002	0.016	0.9026	
AC	0.0036	1	0.0036	0.257	0.6275	
BC	0.0056	1	0.0056	0.4022	0.5461	
A^2	6.09	1	6.09	435.72	< 0.0001	**
B^2	0.7095	1	0.7095	50.73	0.0002	**
C^2	0.5247	1	0.5247	37.52	0.0005	**
Residual	0.0979	7	0.0140			
Lack of fit	0.0050	3	0.0017	0.071	0.9722	Not significant
Pure Error	0.0929	4	0.0232			
Sum	11.59	16				
$R^2 = 0.9916$		$R_{adj}{}^2 = 0.9807$				

** indicates that the result is highly significant, $P < 0.01$

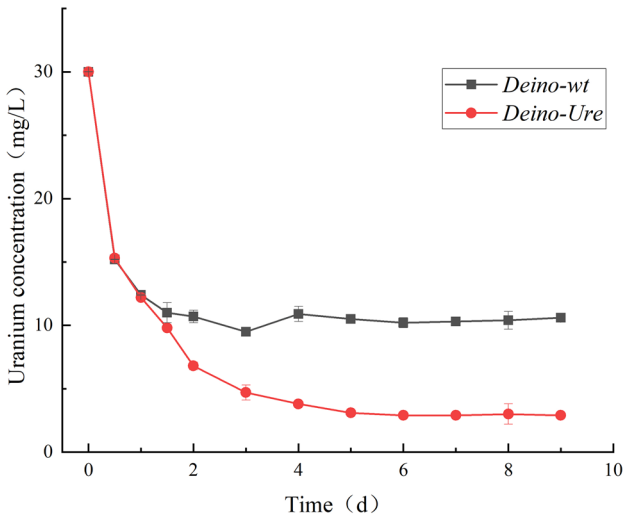

Fig. 9 Effect of time on uranium enrichment in Deino-*wt* and Deino-*Ure*

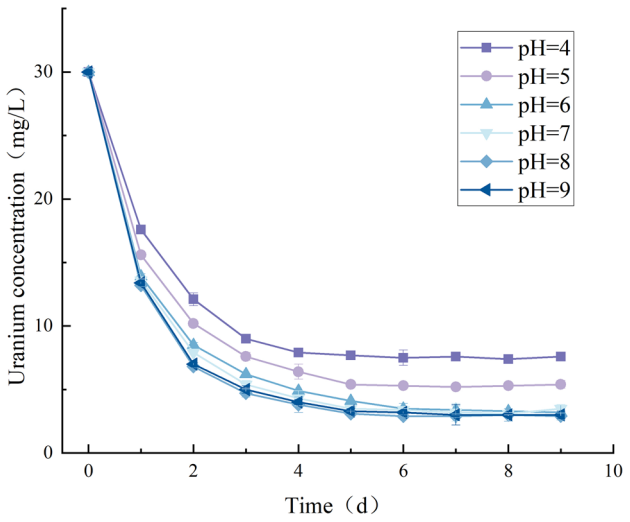

Fig. 10 Effect of pH on uranium enrichment in Deino-*wt* and Deino-*Ure*

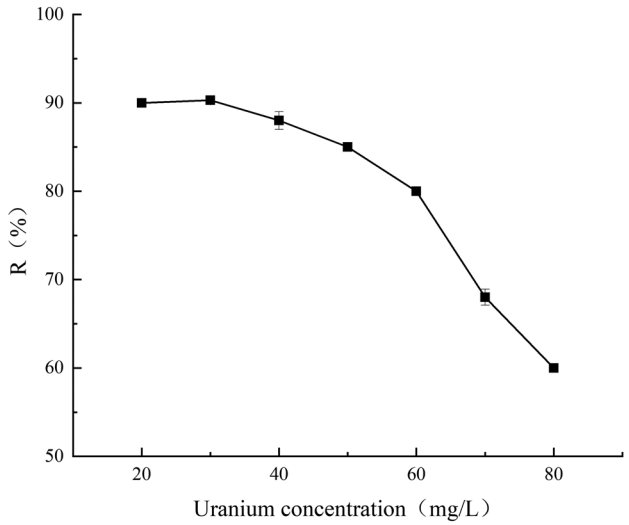

Fig. 11 Effect of uranium initial concentration on uranium enrichment in Deino-*wt* and Deino-*Ure*

were represented as U(IV), elucidating that after Deino-*Ure* mineralized U(VI), its reaction products were coexisting substances of U(IV) and U(VI).

Finally, the composition of the Deino-*Ure*-enriched uranium product was analyzed by X-ray diffraction (XRD), as shown in Fig. 14c. According to the relevant data of the PDF standard card (PDF#72-1937), the characteristic peaks of calcite appeared in the sample, describing that the products after the mineralization of U(VI) by Deino-*Ure* mainly existed in the form of calcite, and combined with the results of SEM, EDS, and XPS analyses of the sample, which inferred that uranium might have co-precipitated with calcium during the mineralization of U(VI) at Deino-*Ure*, forming a stable U(VI)/U(IV)-calcite mineral precipitation.

Table 5 Variance analysis of calcium carbonate yield by response surface model

Source of variance	Sum of square	Degree of freedom	Mean square	F value	*P* value	Significance
Model	11,000.05	9	1222.23	285.66	< 0.0001	**
A:Ni^{2+} concentration	1984.5	1	1984.50	463.82	< 0.0001	**
B:Urea concentration	741.2	1	741.12	173.22	< 0.0001	**
C:Ca^{2+} concentration	28.13	1	28.23	6.57	0.0373	*
AB	4.00	1	4.00	0.9349	0.3658	
AC	64.00	1	64.00	14.96	0.0062	**
BC	6.25	1	6.25	1.46	0.2660	
A^2	5818.87	1	5818.87	1360.00	< 0.0001	**
B^2	457.6	1	457.60	106.95	< 0.0001	**
C^2	1278.44	1	1278.44	298.80	< 0.0001	**
Residual	29.95	7	4.28			
Lack of fit	6.75	3	2.25	0.3879	0.9722	Not significant
Pure Error	23.20	4	5.80			
Sum	11,030.00	16				
$R^2 = 0.9973$		$R_{adj}^2 = 0.9938$				

*Indicates that the result is significant, $0.01 < P < 0.05$ ** indicates that the result is highly significant, $P < 0.01$

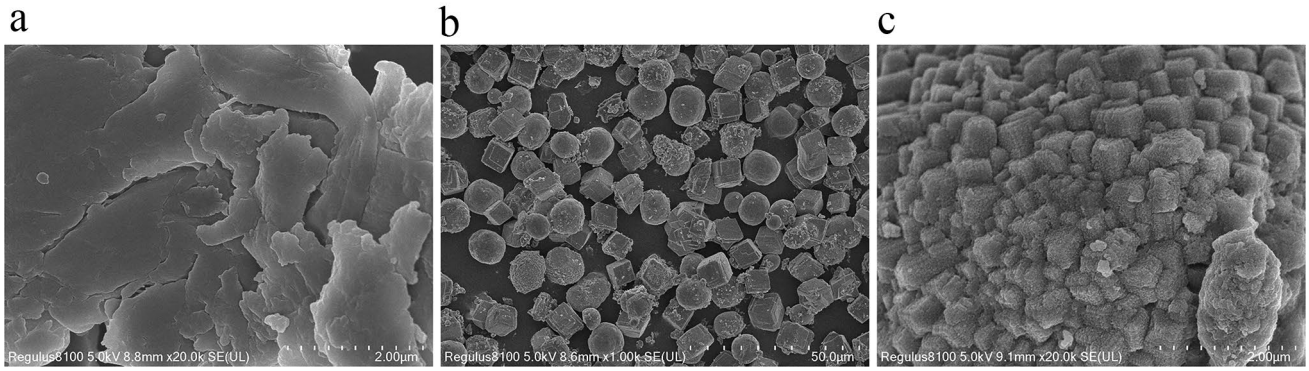

Fig. 12 SEM images before and after uranium mineralization by Deino-*Ure*. (a) SEM image of Deino-*Ure* before mineralization; **b c** SEM images of different multiples after mineralization of Deino-*Ure*

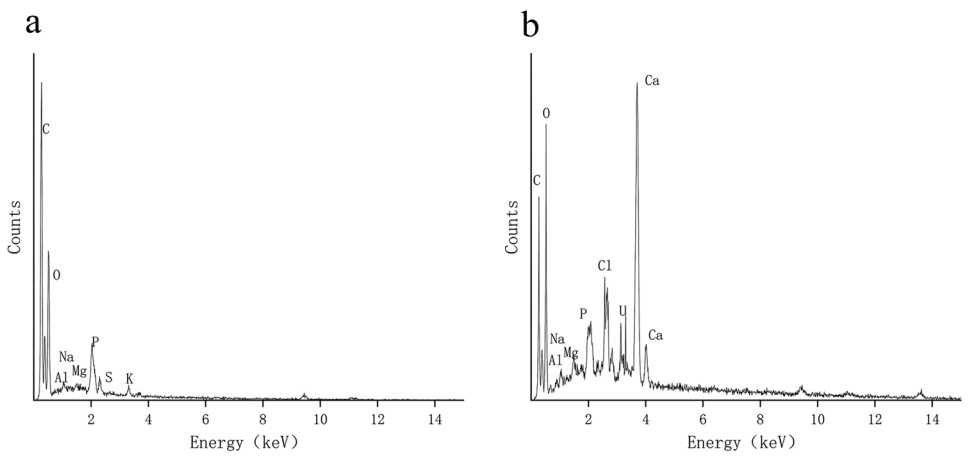

Fig. 13 EDS spectra of U(VI) mineralized by Deino-*Ure*. **a** EDS spectrum of Deino-*Ure* before mineralization of U(VI); **b** EDS spectrum of Deino-*Ure* after mineralization of U(VI)

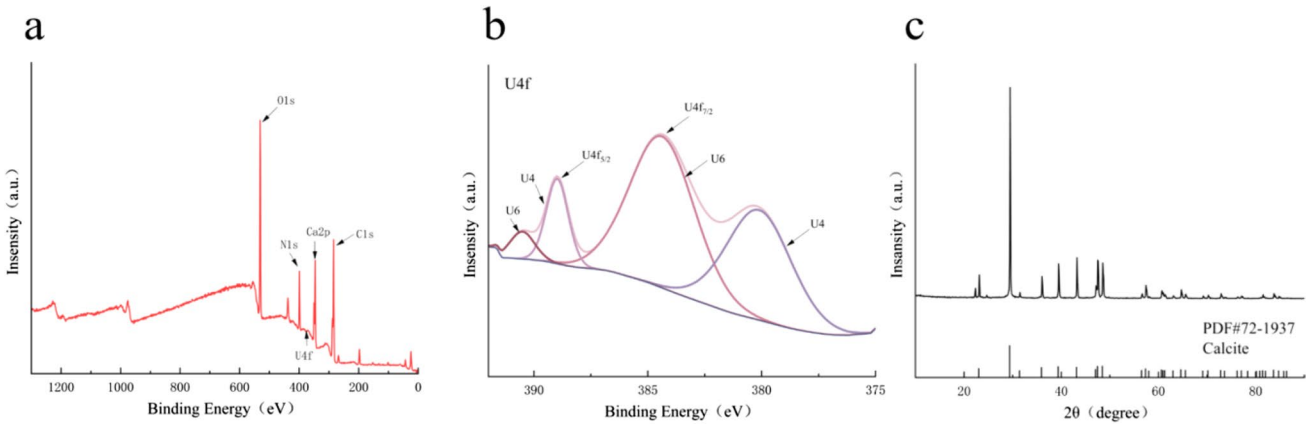

Fig. 14 XPS analysis and XRD pattern of U(VI) mineralized by Deino-*Ure*. **a** Full spectrum of U(VI) mineralized by Deino-*Ure*; **b** U4f spectrum of U(VI) mineralized by Deino-*Ure*; **c** XRD pattern of U(VI) mineralized by *Deino-Ure*

Conclusion

In this study, a genetically engineered bacterium Deino-*Ure* with prominent radiation resistance and mineralization ability was successfully constructed, and the transfer of *Ure* gene did not affect the growth of the proposed bacterium. The urease activity and mineralization ability of Deino-*Ure* were successfully verified, and its urease activity was relatively outstanding under 0.5 mmol/L of Ni^{2+}, 10 g/L of Ca^{2+}, and 30 g/L of urea. After the experimental analysis of the response surface, the optimal concentrations for mineralization of Ni^{2+}, Ca^{2+}, and urea were calculated to be 0.5 mmol/L, 10 g/L, and 35 g/L, respectively. Moreover, the enrichment rate of uranium by Deino-*Ure* could reach 90% when the mineralization time was beyond 7 days, the pH was in the range of 6 ~ 9, and the initial concentration of uranium was 30 mg/L. During the mineralization of U(VI) by Deino-*Ure*, uranium might co-precipitate with calcium to form mineralized crystallization and attachment to the surface of the thallus, forming a stable U(VI)/U(IV)-calcite mineral precipitation. This study provided a new strategy for the remediation of uranium in soil, and the use of genetically engineered bacteria to mineralize uranium into calcite structures, so as to reduce the harmful and toxic effects of uranium in soil on the environment and organisms.

Acknowledgements This work was supported by the Environmental Protection Research Project of Hunan Province (HBKYXM-2023021), the Independent Research Project of the China Academy of Radiation Protection (2022 Platform Project of the National Key Laboratory of Radiation Environment and Health for Environmental Protection -4), the National Natural Science Foundation of China (42377076), the Natural Science Foundation of Hunan Province (2023JJ50129), the Basic Applied Research Special Project of Hengyang (202002042158), and the Hunan Provincial Innovation Foundation for Postgraduates (QL20230242).

Declarations

Conflict of interest We declare that no known conflict of interest that could have appeared to influence the work reported in this paper.

References

1. Liu S, Pan G, Zhang Y, Xu J, Ma R, Shen Z, Dong S (2019) Risk assessment of soil heavy metals associated with land use variations in the riparian zones of a typical urban river gradient. Ecotoxicol Environ Saf 181:435–444. https://doi.org/10.1016/j.ecoenv.2019.04.060
2. Niu Y, Chen F, Li Y, Ren B (2021) Trends and sources of heavy metal pollution in global river and lake sediments from 1970 to 2018. Rev Environ Contam Toxicol 257:1–35. https://doi.org/10.1007/398_2020_59
3. Dhuldhaj UP, Singh R, Singh VK (2023) Pesticide contamination in agro-ecosystems: toxicity, impacts, and bio-based management strategies. Environ Sci Pollut Res Int 30:9243–9270. https://doi.org/10.1007/s11356-022-24381-y
4. Qin G, Niu Z, Yu J, Li Z, Ma J, Xiang P (2021) Soil heavy metal pollution and food safety in China: effects, sources and removing technology. Chemosphere 267:129205. https://doi.org/10.1016/j.chemosphere.2020.129205
5. Foong SY, Cheong KY, Kong SH, Yiin CL, Yek PNY, Safdar R, Liew RK, Loh SK, Lam SS (2023) Recent progress in the production and application of biochar and its composite in environmental biodegradation. Biores Technol 387:129592. https://doi.org/10.1016/j.biortech.2023.129592
6. Ma M, Wang R, Xu L, Xu M, Liu S (2020) Emerging health risks and underlying toxicological mechanisms of uranium contamination: lessons from the past two decades. Environ Int 145:106107. https://doi.org/10.1016/j.envint.2020.106107
7. Adeola AO, Iwuozor KO, Akpomie KG, Adegoke KA, Oyedotun KO, Ighalo JO, Amaku JF, Olisah C, Conradie J (2023)

Advances in the management of radioactive wastes and radionuclide contamination in environmental compartments: a review. Environ Geochem Health 45:2663–2689. https://doi.org/10.1007/s10653-022-01378-7
8. Yuan Y, Xiang M, Liu C, Theng BKG (2019) Chronic impact of an accidental wastewater spill from a smelter, China: a study of health risk of heavy metal(loid)s via vegetable intake. Ecotoxicol Environ Saf 182:109401. https://doi.org/10.1016/j.ecoenv.2019.109401
9. Cordova-Marks FM, Carson WO, Monetathchi A, Little A, Erdrich J (2022) Native and indigenous populations and gastric cancer: a worldwide review. Int J Environ Res Public Health. https://doi.org/10.3390/ijerph19095437
10. Cheng C, Chen L, Guo K, Xie J, Shu Y, He S, Xiao F (2022) Progress of uranium-contaminated soil bioremediation technology. J Environ Radioact 241:106773. https://doi.org/10.1016/j.jenvrad.2021.106773
11. Azhar U, Ahmad H, Shafqat H, Babar M, Shahzad Munir HM, Sagir M, Arif M, Hassan A, Rachmadona N, Rajendran S, Mubashir M, Khoo KS (2022) Remediation techniques for elimination of heavy metal pollutants from soil: a review. Environ Res 214:113918. https://doi.org/10.1016/j.envres.2022.113918
12. Rajasekar A, Wilkinson S, Moy CKS (2021) MICP as a potential sustainable technique to treat or entrap contaminants in the natural environment: a review. Environ Sci Ecotechnol 6:100096. https://doi.org/10.1016/j.ese.2021.100096
13. Peng D, Qiao S, Luo Y, Ma H, Zhang L, Hou S, Wu B, Xu H (2020) Performance of microbial induced carbonate precipitation for immobilizing Cd in water and soil. J Hazard Mater 400:123116. https://doi.org/10.1016/j.jhazmat.2020.123116
14. Khadim HJ, Ammar SH, Ebrahim SE (2019) Biomineralization based remediation of cadmium and nickel contaminated wastewater by ureolytic bacteria isolated from barn horses soil. Environ Technol Innov. https://doi.org/10.1016/j.eti.2019.100315
15. De Muynck W, De Belie N, Verstraete W (2010) Microbial carbonate precipitation in construction materials: a review. Ecol Eng 36:118–136. https://doi.org/10.1016/j.ecoleng.2009.02.006
16. Frederik H, Verstraete W (2002) Key roles of pH and calcium metabolism in microbial carbonate precipitation. Rev Environ Sci Biotechnol 1:3–7. https://doi.org/10.1023/A:1015135629155
17. Pei D, Liu Z, Wu W, Hu B (2021) Transcriptome analyses reveal the utilization of nitrogen sources and related metabolic mechanisms of *Sporosarcina pasteurii*. PLoS ONE 16:e0246818. https://doi.org/10.1371/journal.pone.0246818
18. Onal Okyay T, Frigi Rodrigues D (2013) High throughput colorimetric assay for rapid urease activity quantification. J Microbiol Methods 95:324–326. https://doi.org/10.1016/j.mimet.2013.09.018
19. Šovljanski O, Tomić A, Markov S (2022) Relationship between bacterial contribution and self-healing effect of cement-based materials. Microorganisms. https://doi.org/10.3390/microorganisms10071399
20. Chen HJ, Chang HL, Tang CW, Yang TY (2022) Application of biomineralization technology to self-healing of fiber-reinforced lightweight concrete after exposure to high temperatures. Materials. https://doi.org/10.3390/ma15217796
21. Tamaddon F, Arab D (2019) Urease covalently immobilized on cotton-derived nanocellulose-dialdehyde for urea detection and urea-based multicomponent synthesis of tetrahydro-pyrazolopyridines in water. RSC Adv 9:41893–41902. https://doi.org/10.1039/c9ra05240b
22. Basu B (2022) The radiophiles of Deinococcaceae family: resourceful microbes for innovative biotechnological applications. Current Res Microbial Sci 3:100153. https://doi.org/10.1016/j.crmicr.2022.100153
23. Liang L, Heveran C, Liu R, Gill RT, Nagarajan A, Cameron J, Hubler M, Srubar WV 3rd, Cook SM (2018) Rational control of calcium carbonate precipitation by engineered *Escherichia coli*. ACS Synth Biol 7:2497–2506. https://doi.org/10.1021/acssynbio.8b00194
24. Juminaga D, Baidoo EE, Redding-Johanson AM, Batth TS, Burd H, Mukhopadhyay A, Petzold CJ, Keasling JD (2012) Modular engineering of L-tyrosine production in *Escherichia coli*. Appl Environ Microbiol 78:89–98. https://doi.org/10.1128/aem.06017-11
25. Xia Z, Xiaoran J, Jie G, Jiahua B, Lunjie W, Yao N, Yan X (2022) Gene mining of urease and recombinant expression in *Bacillus subtilis*. J Food Sci Biotechnol 41:28–37. https://doi.org/10.3969/j.issn.1673-1689.2022.05.004
26. Liu Q, Jin X, Fang F, Li J, Du G, Kang Z (2019) Food-grade expression of an iron-containing acid urease in *Bacillus subtilis*. J Biotechnol 293:66–71. https://doi.org/10.1016/j.jbiotec.2019.01.012
27. Salis HM, Mirsky EA, Voigt CA (2009) Automated design of synthetic ribosome binding sites to control protein expression. Nat Biotechnol 27:946–950. https://doi.org/10.1038/nbt.1568
28. Chen J, Zhu R, Zhou J, Yang T, Zhang X, Xu M, Rao Z (2021) Efficient single whole-cell biotransformation for L-2-aminobutyric acid production through engineering of leucine dehydrogenase combined with expression regulation. Biores Technol 326:124665. https://doi.org/10.1016/j.biortech.2021.124665
29. Whiffin VS (2004) Microbial $CaCO_3$ precipitation for the production of biocement. Murdoch University,
30. Weatherburn MW (1967) Phenol-hypochlorite reaction for determination of ammonia. Anal Chem 39:971–974
31. Qiuli L, Xiaoping L (2022) Spectrophotometric determination for the total uranium in high-level liquid waste. World Nucl Geosci 39:124–129. https://doi.org/10.3969/j.issn.1672-0636.2022.01.013
32. Alfano M, Cavazza C (2020) Structure, function, and biosynthesis of nickel-dependent enzymes. Protein Sci A Publ Protein Soc 29:1071–1089. https://doi.org/10.1002/pro.3836
33. Mazzei L, Musiani F, Ciurli S (2020) The structure-based reaction mechanism of urease, a nickel dependent enzyme: tale of a long debate. J Biol Inorg Chem JBIC Publ Soc Biol Inorg Chem 25:829–845. https://doi.org/10.1007/s00775-020-01808-w
34. Wang C, Hao L, Sun X, Yang Y, Yin Q, Li M (2022) Response mechanism of psychrotolerant Bacillus cereus D2 towards Ni (II) toxicity and involvement of amino acids in Ni (II) toxicity reduction. J Hazard Mater 430:128363. https://doi.org/10.1016/j.jhazmat.2022.128363
35. Bellouard M, Gasser M, Lenglet S, Gilardi F, Bararpour N, Augsburger M, Thomas A, Alvarez JC (2022) Toxicity and metabolomic impact of cobalt, chromium, and nickel exposure on HepaRG hepatocytes. Chem Res Toxicol 35:807–816. https://doi.org/10.1021/acs.chemrestox.1c00429
36. Okwadha GD, Li J (2010) Optimum conditions for microbial carbonate precipitation. Chemosphere 81:1143–1148. https://doi.org/10.1016/j.chemosphere.2010.09.066
37. Mengyao G, Jingfang W (2020) Research status on preparation and transformation of *E. coli* competent cell. J Hebei North Univ 36:44–48. https://doi.org/10.3969/j.issn.1673-1492.2020.08.017
38. Pan S, Ryu SY, Sheu SS (2011) Distinctive characteristics and functions of multiple mitochondrial Ca_{2+} influx mechanisms. Sci China Life Sci 54:763–769. https://doi.org/10.1007/s11427-011-4203-9

39. Xiao Y, Yin X, Zing M (2020) Research advance on molecular mechanism of apoptosis induced by heavy metal-associated calcium overload. Pract Prev Med 27:252–257. https://doi.org/10.3969/j.issn.1006-3110.2020.02.036
40. Walkon LL, Strubbe-Rivera JO, Bazil JN (2022) Calcium overload and mitochondrial metabolism. Biomolecules. https://doi.org/10.3390/biom12121891
41. Frankenberger WTF, Johanson JB (1982) Effect of pH on enzyme stability in soils. Soil Biol Biochem 14:433–437. https://doi.org/10.1016/0038-0717(82)90101-8